Iran Polym J (2013) 22:155–163
DOI 10.1007/s13726-012-0114-2

ORIGINAL PAPER

Effect of MCM-41 nanoparticles on the kinetics of free radical and RAFT polymerization of styrene

Mohammadreza Sarsabili · Mehdi Parvini · Mehdi Salami-Kalajahi · Abbas Asfadeh

Received: 12 August 2012 / Accepted: 12 December 2012 / Published online: 21 December 2012

Abstract To examine the effect of mobil composition of matter 41 (MCM-41) nanoparticles on the kinetics of free radical and 2-(dodecylthiocarbonothioylthio)-2-methyl-propionic acid (DDMAT)-mediated reversible addition fragmentation chain transfer (RAFT) polymerization, the polymerization reaction using various amounts of as-synthesized MCM-41 were performed. To study the reaction kinetics, conversion, molecular weight and polydispersity index (PDI) were obtained during the polymerization. Also, differential scanning calorimetry (DSC) was used to determine the glass transition temperature (T_g) values of samples. According to the results, in free radical polymerization, conversion was increased by adding nanoparticles but the reverse trend was observed in RAFT polymerization. The same results were obtained for molecular weight values. In free radical polymerization, increasing the MCM-41 content led to higher PDI value, while in RAFT polymerization it did not appreciably affect the PDI value. In RAFT polymerization, no induction time was observed which indicates that DDMAT is an appropriate RAFT agent for styrene polymerization. Also in free radical polymerization, the addition of MCM-41 particles reduced T_g values in comparison to neat PS. On the other hand, there was an increase in T_g value up to 5 wt% of MCM-41 loading and a drastic reduction was observed in 7 wt% MCM-41 loading in the RAFT polymerization. Finally, the T_g values of nanocomposites produced by RAFT method were higher than those in the nanocomposites synthesized using the free radical method.

Keywords MCM-41 · Nanocomposite · Kinetics · Reversible addition fragmentation chain transfer (RAFT) polymerization · Molecular weight distribution (MWD) · Differential scanning calorimetry (DSC)

M. Sarsabili · M. Parvini (✉)
Department of Chemical Engineering, Gas, and Petroleum, Semnan University, PO Box: 35131-19111, Semnan, Iran
e-mail: m.parvini@sun.semnan.ac.ir

M. Salami-Kalajahi
Department of Polymer Engineering, Sahand University of Technology, PO Box: 51335-1996, Tabriz, Iran

M. Salami-Kalajahi
Institute of Polymeric Materials, Sahand University of Technology, PO Box: 51335-1996, Tabriz, Iran

A. Asfadeh
Department of Polymer Engineering and Color Technology, Amirkabir University of Technology, PO Box: 15875-4413, Tehran, Iran

Introduction

Incorporation of particles, mainly layered silicates [1, 2], nanotubes [3, 4], and spherical silica particles [5, 6], into organic polymeric materials has been the subject of growing interest in different technological innovations. These hybrid materials have been used in gas separation process [7], flame retardants [8], reinforced composite materials [9, 10] and other high demanding materials with improved electrical [11, 12] or mechanical properties [13, 14]. Since the first report of synthesizing mesoporous silica by scientists of Mobil Oil Company [15, 16] in 1992, it has attracted attention of both industry and academia due to their diverse potential applications; including catalysis [17], filtration [18], chromatography [19], etc. The most well-known type of this class of materials is mobil composition of matter 41(MCM-41). The MCM-41 has attracted scientists' attention due to its good thermal stability, very large void fraction which can affect the kinetics of reaction, rather low density

and finally having hydroxyl functional active sites [20, 21]. Although MCM-41 particles display a high potential applicability in different fields, the important subject is their effect on polymerization kinetics and subsequently the yield of reaction and properties of obtained polymer. In this regard, there are some studies on the effect of MCM-41 as catalyst support on the polymerization of polyolefins [22, 23].

To achieve optimum control over the structure of inorganic/organic hybrid materials, controlled/living radical polymerization (CLRP) techniques are preferred for providing relatively facile synthesis of well-defined polymers [24]. In comparison with other CLRP techniques, reversible addition fragmentation chain transfer (RAFT) polymerization has superior advantages such as good compatibility with a wide range of monomers and facile experimental conditions that are similar to conventional radical polymerization [25, 26]. The synthesis of well-defined nanocomposites containing mesoporous silica particles is a matter of concern since the kinetics of polymerization is directly influenced by nanoparticles [27]. Although there are some reports on the effect of different nanoparticles on polymerization kinetics [3, 25, 27, 30–33], there is no report on the effect of MCM-41 nanoparticles on reaction kinetics. In some research works, the effect of nanoparticles on RAFT polymerization has been studied and the RAFT agent has been found inappropriate for styrene or methyl methacrylate systems [2, 25]. In this respect, we investigated the effect of MCM-41 on the kinetics of polymerization and molecular weight distribution in both free radical and RAFT polymerization of styrene with an appropriate RAFT agent. To the best of our knowledge, this is the first report of kinetic study of RAFT polymerization in the presence of MCM-41 while comparisons are made with free radical polymerization.

Experimental

Materials

Styrene (Aldrich, 99 %) was passed through a basic alumina column and dried over calcium hydride before use. Azobisisobutyronitrile (AIBN, Acros) was recrystallized from methanol. The obtained AIBN was dried under vacuum at the pressure of 0.1 mbar. Tetrahydrofuran (THF, Merck, 99 %), ammonium solution (Merck, 25 wt%), ethanol (Merck, 99 %), cetyltrimethylammonium bromide (CTAB, Merck), tetraethoxysilane (TEOS, Merck), dicyclohexylcarbodiimide (DCC, Acros), 4-dimethylaminopyridine (DMAP, Merck), acetone (Merck, EMPLURA®), chloroform (Merck, EMPLURA®), hydrochloric acid (Merck, 37 %), 1-dodecanethiol (Riedel-de Haen, 99 %), carbon disulfide (Fluka, >99 %) and magnesium sulfate (Dae-Jung) were used as received without further purification.

Preparation of MCM-41 nanoparticles

MCM-41 particles were synthesized as reported in literature [28]. CTAB (5.010 g, 1.37×10^{-2} mol) was dissolved in 100 mL of deionized water and stirred vigorously for 5 min until the solution became homogeneous and clear. Then 37.4 mL of ammonium solution (25 wt%) was added slowly to the CTAB solution to form gel-like mixture. After 10 min stirring at room temperature, a freshly diluted solution of ethanol (152 mL) was added and the solution was stirred for 20 min. Then, TEOS (10.2 mL, 2.99×10^{-5} mol) was added dropwise during 30 min and stirred for 3 h vigorously. The white powder (5.707 g) was precipitated, filtered, and washed with deionized water several times for extracting the by-products and then dried in vacuum oven at 110 °C for 48 h. To remove CTAB, the dried white powder was calcinated at 550 °C for 6 h and finally 3.564 g MCM-41 nanoparticles were obtained.

Preparation of 2-(dodecylthiocarbonothioylthio)-2-methylpropionic acid (DDMAT)

DDMAT was synthesized according to the previously reported procedure [29]. 1-Dodecanethiol (40.400 g, 0.20 mol), acetone (0.12 g, 1.655 mol), and CTAB (3.245 g, 0.0089 mol) were added into a 250 mL round-bottom flask equipped with mechanical stirrer and stirred for 5 min at 12.5 °C. Sodium hydroxide solution (50 %) (16.800 g, 0.21 mol) was added dropwise over 10 min and then the mixture was stirred for additional 20 min. Afterwards, the solution of carbon disulfide (12.1 mL, 0.20 mol) in acetone (0.02 mL, 0.345 mol) was added over 30 min (caution: CS_2 is highly pungent). At this stage, the color changed from an opaque milky white to yellow. Ten minutes later, chloroform (24.2 mL, 0.3 mol) was added in one portion, followed by dropwise addition of 50 % sodium hydroxide solution (40.000 g) over 40 min. The mixture was stirred overnight with mechanical stirrer. Then, the solution was filtered and washed thoroughly with acetone. Acetone was removed under reduced pressure and a yellow powder was obtained which was dissolved in deionized water (200 mL) and then participated by adding 30 mL of HCl (37 %). DDMAT was collected by filtration and dried under reduced pressure. Then, DDMAT was dissolved in 400 mL of *n*-hexane and the solution was dried over anhydrous $MgSO_4$ and filtered to remove the by-products. DDMAT was recrystallized from the solution, filtered and dried under vacuum (12.000 g, yield: 32.9 %).

^{1}H NMR (in $CDCl_3$): 0.89 ppm (t, 3 H), 1.30–1.5 ppm (m, 18 H), 1.6–1.7 ppm (m, 2 H), 1.7–1.8 ppm (s, 6 H), 3.2 ppm (t, 2 H), 11.0 ppm (s, 1 H).

FTIR: 2,849 cm^{-1}(CH), 1,716 cm^{-1}(C=O), 1,069 cm^{-1} (C=S), 814 cm^{-1}(C–S).

Polymerization of styrene via free radical and RAFT polymerizations

Free radical and RAFT polymerizations of styrene were carried out through glass vials. For this purpose, the polymerization reactions containing various amount of particles and RAFT agent were performed during 12 h for free radical and 18 h for RAFT systems. In a typical procedure, various amounts of dried MCM-41 nanoparticles (from 1 to 9 wt% relative to monomer) along with RAFT agent (4.38 mmol, 1.600 g, in RAFT polymerization) in a known quantity of styrene monomer (0.5 mol, 50 mL) was dispersed and AIBN (0.871 mmol, 0.143 g) was added into a 250-mL lab reactor and mixed for 2 h until it was converted to homogeneous mixture. Then, the reactor's contents were equally transferred into the glass vials and then degassed under the nitrogen atmosphere, sealed and placed in an oil bath at 70 °C. The polymerizations were stopped by cooling the reaction mixture in ice water after definite time periods. The cool methanol was used for polymer precipitation. After weighing procedures, the samples were put into vacuum oven for removing volatile components. Recipes of different polymerization reactions are shown in Table 1.

Separation of polymer chains from particles

The prepared nanocomposites were dissolved in THF and the polymer chains were separated from MCM-41 particles by high-speed ultracentrifugation (10,000 rpm).The solution was passed through a 0.2 μm regenerated cellulose (RC) filter and then poured into methanol (500 mL) to precipitate polymer chains. After filtration, the polymer was dried overnight in a vacuum oven at temperature 50 °C.

Instrumentation

FTIR spectra were recorded on a Bomem FTIR spectrophotometer, within a range of 500–4,000 cm^{-1} using a resolution of 4 cm^{-1}. An average of 32 scans has been reported for each sample. The cell path length was kept constant in all experiments. The samples were prepared on a KBr pellet in vacuum desiccators under a pressure of 0.01 torr. Ultrasonication was performed by an ultrasound probe (Hielscher UIP1000hd, 20 kHz, Germany). Average molecular weights and molecular weight distributions were measured by gel permeation chromatography (GPC) technique. An Agilent 1,100 series with a set of columns of pore sizes of 1,000 Å was utilized to determine polymer average molecular weight and polydispersity index (PDI). THF was used as an eluent at a flow rate of 1.0 mL min^{-1}, and the calibration was carried out using low polydispersity polystyrene standards. Thermal analyses were carried out using a differential scanning calorimetry (DSC) instrument (Netzsch DSC 200 F3, Netzsch Co, Selb/Bavaria, Germany). Nitrogen at a rate of 50 mL min^{-1} was used as the purging gas. Aluminum pans containing 2–3 mg of the samples were sealed using the DSC sample press. The samples were heated from ambient temperature to 180 °C at a heating rate of 10 °C/min. Glass transition temperature (T_g) was obtained as the inflection point of the heat capacity jump. Transmission electron microscope (TEM), FEG Philips CM, with an accelerating voltage of 200 kV was used. Surface morphology of powder samples was examined by scanning electron microscope (SEM: Philips XL30) with acceleration voltage of 20 kV. Spectroscopic characterization by H NMR was performed at room temperature with a Bruker 300 MHz instrument using $CDCl_3$ as solvent. Materials porosity was characterized by N_2 adsorption/desorption curves obtained with a Quntasurb QS18 (Quntachrom) apparatus. The surface area and pore size distribution values were obtained with the corrected BET equation and Broekhoff and de Boermodels, respectively.

Table 1 The recipes of PS/MCM-41 nanocomposites prepared via in situ free radical and RAFT polymerization systems at 70 °C

Sample code	MCM-41 content (wt%)	Polymerization system
FP0	0	Free radical
FP3	3	Free radical
FP5	5	Free radical
FP7	7	Free radical
FP9	9	Free radical
RP0	0	RAFT
RP3	3	RAFT
RP5	5	RAFT
RP7	7	RAFT

Results and discussion

MCM-41 characteristics

As it may be observed in Fig. 1, SEM image of synthesized MCM-41 particles shows that majority of particles are spherical with diameter ranging from 200 to 700 nm. High specific surface area (~1,162 m^2 g^{-1}) and nanoscale pore size (~3 nm), which have been obtained by isothermal nitrogen adsorption–desorption indicate that spherical particles are highly porous as expected. Moreover, as shown in Fig. 2, TEM image of MCM-41 supports the above results. The regular channels and cylindrical structure with equal lengths are shown, which confirm the preparation of ordered MCM-41 particles. The MCM-41 nanoparticles with average pore size of approximately

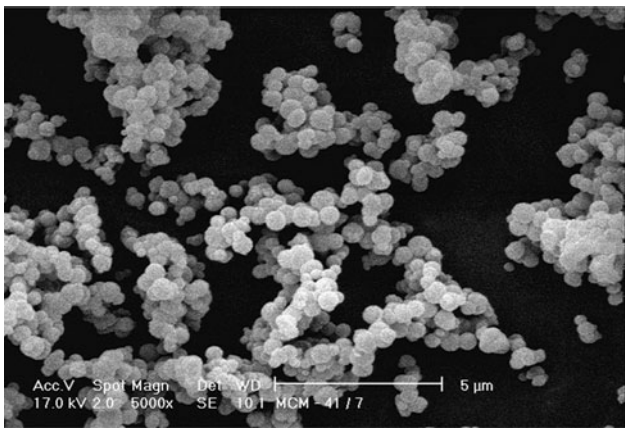

Fig. 1 SEM image of MCM-41 particles

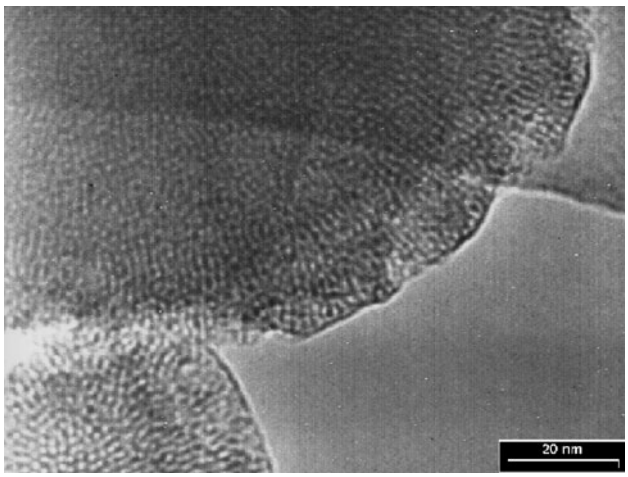

Fig. 2 TEM image of MCM-41 particles

2.1 nm were prepared by hydrolysis and condensation of TEOS in the presence of CTAB micelles as cationic surfactant. The MCM-41 nanoparticles exhibit very high specific surface area and internal pore volume as reported in Table 2.

Polymerization kinetics

In all experiments, the molar concentration of initiator (and DDMAT in RAFT polymerization experiments) was kept constant while various amounts of MCM-41 particles, including 0, 3, 5, 7, and 9 wt% relative to monomer, were used. Figure 3a depicts monomer conversion versus free radical polymerization time. The maximum polymerization rate can be observed at 7 wt% of MCM-41, and then further increasing of the MCM-41 particles amount to 9 wt% leads to reduction in the rate of monomer consumption. In initial stages of the reactions, the particles exert little effect on the reaction kinetics; however, at higher conversions, increasing silica content leads to an increase of the polymerization rate. This is attributed to induction of partial polarization of

Table 2 Characteristics of synthesized MCM-41 nanoparticles

S_{sp}^{a} (m^2 g^{-1})	V_g^{b} (cm^3 g^{-1})	Pore diameter[c] (nm)
1,162	0.9	2.1

[a] Specific surface area, measured via BET

[b] Pore specific volume at $p/p^0 = 0.98$, measured via BET

[c] Calculated via BET

the system which can enhance the rate of polymerization [30]. The polar hydroxyl groups on both surfaces and inside the pores of MCM-41 particles are most likely to induce polarity changes of the reaction medium. Also, presence of particles reduces termination reactions due to increasing viscosity. Slower polymerization rate at higher amount of particles has been attributed to lower stability of the system due to the formation of aggregates [31]. With the presence of agglomerated particles in the polymerization system, the radicals are compelled to move in any available space for finding other free radicals and monomers. Thus, the radicals are forced to overcome resistance against reagents and agglomerated silica. Therefore, in a medium with high degree of agglomerated silica, the movement of macro radicals is suppressed which leads to decrement of polymerization rate and conversion. In contrast with free radical polymerization, the rate of polymerization tends to decrease by increased amount of MCM-41 particles in RAFT polymerization (Fig. 3b). Since the concentration of RAFT agent is identical in all the experimental tests, this phenomenon can be attributed to physical absorption of R-ended chains due to the formation of hydrogen bonds or reaction between hydroxyl groups of MCM-41 and carboxyl group of RAFT agent. Extreme affinity of carboxyl group of DDMAT toward OH groups of particles forces the leaving group to link to hydroxyl groups of the MCM-41 particles. As a consequence the leaving group radicals re-initiate polymerization even more slowly. Also, physical absorption takes place for chains initiated with R group and increasing the particle quantity highlights this effect [32]. However, by increasing the chain lengths, the tendency of carboxyl-terminated macro species to be absorbed on the surface of particles is decreased as they become more lipophilic. In some RAFT polymerization reactions, an induction period is observed on logarithm conversion diagram [33, 34]. However, DDMAT as RAFT agent which contains appropriate leaving/re-initiator group results in quick re-initiation and the simultaneous growth of the polymer chains with no induction time.

The development of number-average molecular weight (M_n) with conversion is shown in Fig. 4. In free radical polymerization (Fig. 4a), M_n increases with conversion and

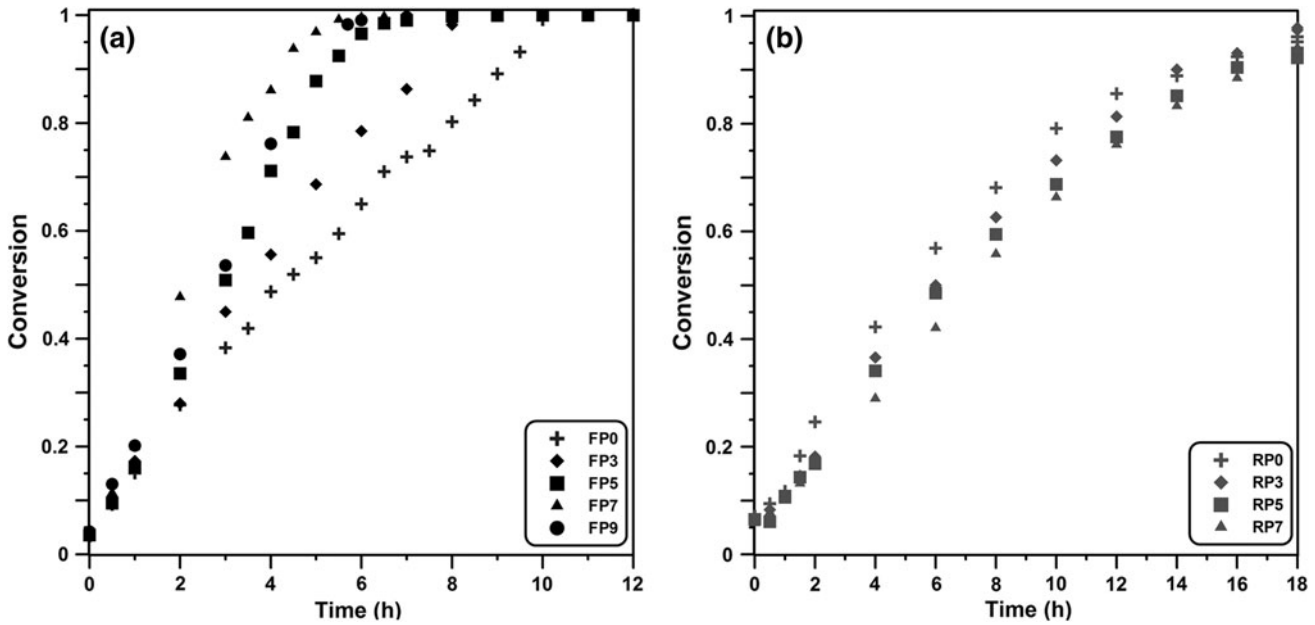

Fig. 3 Conversion versus time for free radical (**a**) and RAFT (**b**) polymerizations of styrene at 70 °C in different contents of as-synthesized MCM-41

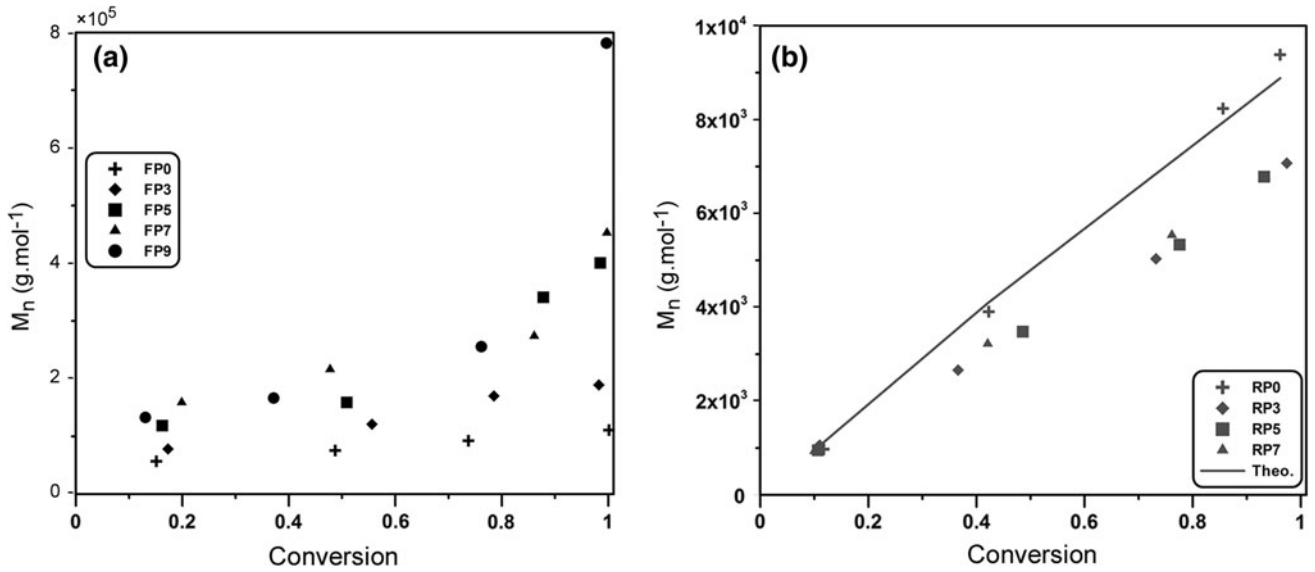

Fig. 4 M_n versus conversion for free radical (**a**) and RAFT (**b**) polymerizations of styrene at 70 °C in different contents of as-synthesized MCM-41

the rate of this increment is faster when higher amounts of MCM-41 particles are used. This is described by the gel effect and diffusive-controlled termination of macroradicals which prolonged the lifetime of macroradicals. As mentioned previously, the presence of particles increases the viscosity of the reaction mixture and reduces the probabilities of termination reactions, which provide greater opportunity for propagation of macroradicals before bimolecular terminations. In RAFT polymerization experiments, M_n increases linearly with conversion which indicates the controlled growth of polymer chains. In a RAFT polymerization, theoretical M_n relates to the conversion via Eq. 1 [35]:

$$\bar{M}_n = \frac{[M]_0 \times \mathrm{MW}_{\mathrm{monomer}}}{[\mathrm{RAFT}]_0} \times X + \mathrm{MW}_{\mathrm{RAFT}} \quad (1)$$

where $[M]_0$ and $[\mathrm{RAFT}]_0$ are initial concentrations of the monomer and RAFT agent, X is the monomer conversion,

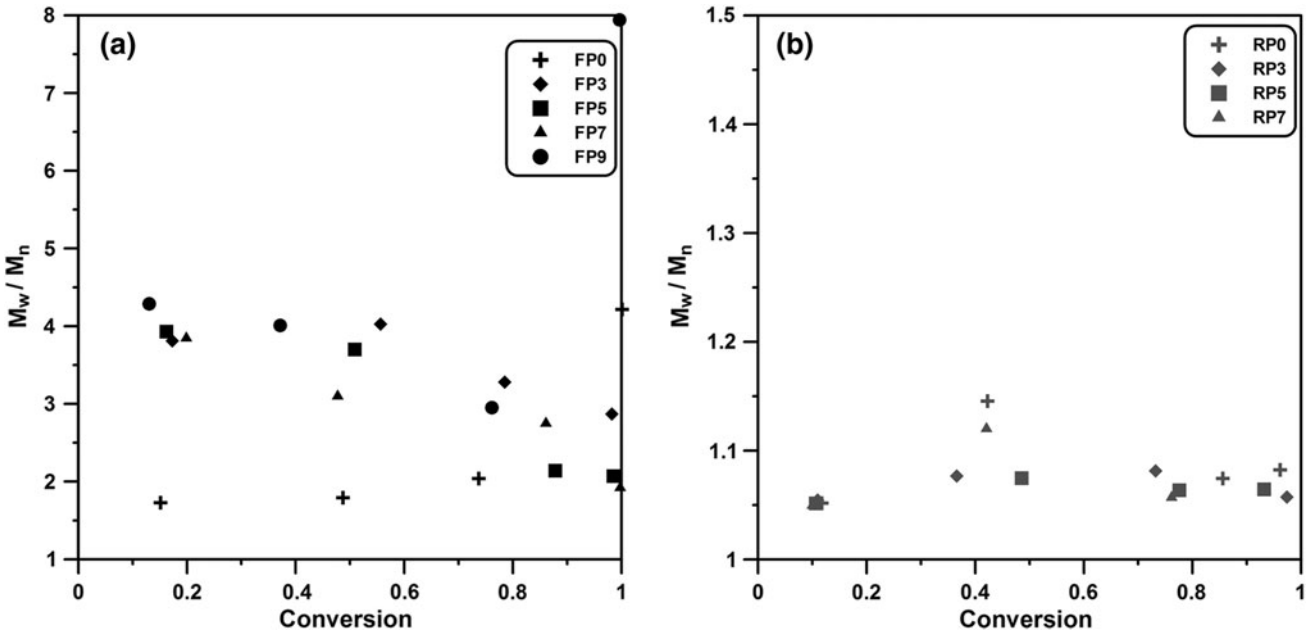

Fig. 5 PDI values versus conversion for free radical (**a**) and RAFT (**b**) polymerizations of styrene at 70 °C in different contents of as-synthesized MCM-41

and $MW_{monomer}$ and MW_{RAFT} are the molecular weights of monomer and RAFT agent.

According to Eq. 1, the rate of increment of M_n is directly affected by initial molar ratio of monomer to RAFT agent. Therefore, it is expected that in all these experimental tests, M_n does not change since the initial molar ratio of monomer to RAFT agent is constant. However, as is observed in Fig. 4, the consistency of theoretical and experimental data is observed only in RP^0 experiment and surprisingly an obvious negative deviation from theoretical values is observed by introducing MCM-41 particles into the polymerization system. This is ascribed to the physical absorption of RAFT agent onto the surface of MCM-41 particles which reduces the mobility of polymer chains and consequently slows down propagation reactions.

Figure 5 represents PDI values versus conversion. In free radical samples, adding MCM-41 particles into the reaction media leads to increment of PDI values. Inappropriate distribution of styrene monomer inside the pores of MCM-41 particles leads to increasing PDI [36]. With addition of the mesoporous silica into the polymerization system, considerable reduction in PDI values is observed with extent of reaction. The reduction is more likely due to the presence of mesopores in MCM-41 structure. It can be seen that at the end of reaction PDI values are considerably increased. The occupied pores by polymer chains and increasing the system viscosity due to MCM-41 particles are the reasons for the above evolving phenomenon. In case of RAFT polymerization, by further conversion, PDI values tend to drop which is an indication of controlled behavior of growing chain. Moreover, with incremental growth of MCM-41 particles PDI does not change considerably and remains under 1.15 in all the tests. This could be due to the appropriate control of polymerization reaction by RAFT agent. RAFT agent leads to a significant decrease in the rate of polymerization and molecular weight of polymer chains. However, a good control of reaction kinetics is provided by very low PDI values. Therefore, it is concluded that the mesoporous silica particles have no effect on the PDI in RAFT experiments.

Characterization of PS/MCM-41 nanocomposites

FTIR

Figure 6 illustrates FTIR spectra for MCM-41 and FP7 and RP7 nanocomposites. Three peaks are observed at 457, 1,080, and 3,423 cm^{-1} in pristine MCM-41 spectrum, which are attributed to Si–O–Si, Si–O–Si and Si–OH groups, respectively. In the spectra of FP7 and RP7 samples, peaks at wavenumbers 3,080, 2,848, 2,918, 1,600, 1,491, 1,060, 1,020, 750, and 696 cm^{-1}, in the order given correspond to polystyrene C–H aromatic stretching vibration, C–H asymmetric stretching vibration of CH_2, C–H symmetric stretching vibration of CH_2, C–C stretching frequency (ring-in-plane), C–H stretching vibration (ring-in-plane), C–H bending vibration (ring-in-plane) and C–H ring out-of-plane bending vibration. Also, in case of RP7

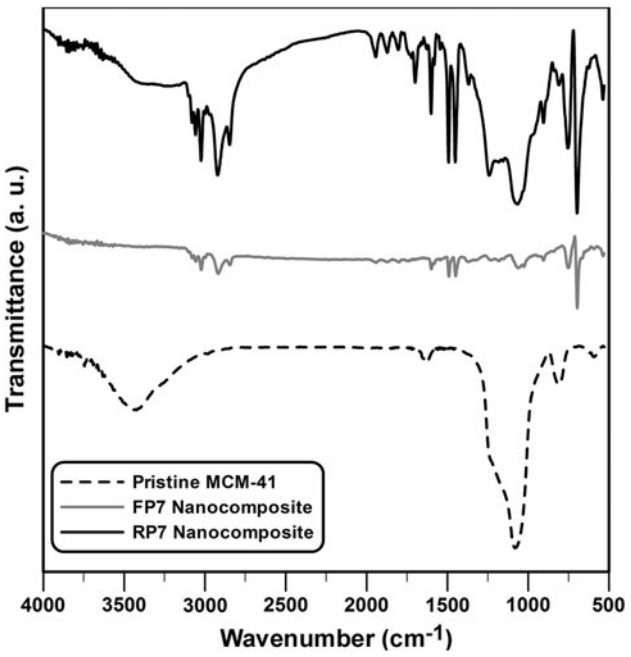

Fig. 6 FTIR spectra of pristine MCM-41 nanoparticles, FP7, and RP7 nanocomposites

sample, the peaks at wavenumbers 1,723 and 1,066 cm^{-1} are related to C=O and C=S groups of RAFT agent, respectively.

Thermophysical properties

Effect of particles on chain confinement has been investigated by means of variation in T_g. Figure 7a shows the DSC thermograms of the samples which are obtained via free radical polymerization. It can be observed that the synthesized nanocomposites have lower T_g values than neat polystyrene. Changes in molecular weight, tacticity and cross-linking density are some reasons behind reduced T_g values [37]. The results indicate that the interaction between the polymer chains and particle surface is significant which has led to formation of nanolayer around the nanoparticle surfaces. Evaluation of the effects of MCM-41 nanoparticle on T_g for the present system is not straightforward. Some authors have disclosed reduction in T_g [38]. With regards to the theory revealed by Tsagarapoulos et al. [39], the reduction of T_g in the nanocomposites synthesized via the free radical polymerization can be attributed to weak interactions between the hydroxyl-containing MCM-41 particles and non-polar polystyrene chains. Nanocomposites obtained via the RAFT polymerization (Fig. 7b) show different trend. By increasing of MCM-41 particles up to 5 wt%, T_g increases but reduces dramatically with further increment of particles content. The observed ascendant trend on T_g up to 5 wt% can be attributed to the formation of hydrogen-bonds between the carboxylic acid chain ends of polymer and hydroxyl groups of MCM-41. This may be also the main reason that the T_g values of nanocomposites prepared by RAFT method are higher than those prepared by free radical polymerization. A high content of MCM-41 leads to aggregation of polymer chains around MCM-41 surface and formation of nanoscale layers. As a consequence, T_g is reduced which does allow more movement of other chains as a result of bigger space [38]. The nanocomposites synthesized by RAFT polymerization method have lower molecular weights than those produced by free radical polymerization method. However,

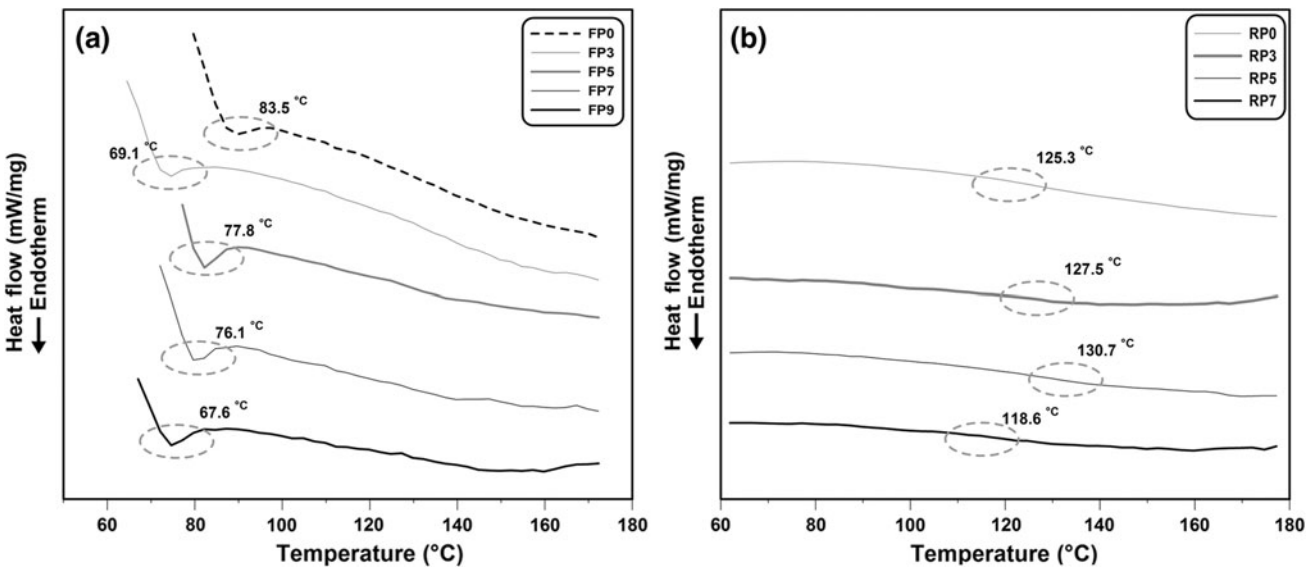

Fig. 7 DSC curves for PS/MCM-41 nanocomposites prepared via free radical (**a**) and RAFT (**b**) polymerization at 70 °C in different contents of nanoparticles

as observed they show much higher T_g values. This can be attributed to both higher PDI values for the nanocomposites synthesized by free radical polymerization and formation of strong hydrogen-bonding between the polymer chains synthesized by RAFT polymerization.

Conclusion

To study the effect of MCM-41 particles on styrene polymerization kinetics, the methods of free radical and RAFT polymerization were performed at 70 °C with various amounts of particles. In free radical polymerization, there was higher conversion observed with increase in MCM-41 particle content up to 7 wt%, but by addition of particles up to 9 wt% the conversion was slowed down. However, in RAFT polymerization method, the rate and conversion rate increased with lower MCM-41 particle content. In samples synthesized by RAFT polymerization method, the M_n followed a linear ascending trend versus higher conversion due to living characteristics of RAFT polymerization. Also, increased particle content resulted in higher M_n among the nanocomposites synthesized by free radical method whereas, a reverse trend was observed for nanocomposites produced by RAFT polymerization. In free radical polymerization system, addition of MCM-41 particles into the polymer system resulted in higher PDI values. However, in RAFT polymerization, the presence of MCM-41 particles has had no effect on PDI values (<1.2). In free radical polymerization, T_g values of the samples were lower than neat polystyrene. However, in samples obtained by RAFT, the T_g increased with higher MCM-41 content up to 5 wt% and, subsequently, with further increase in particle content up to 7 wt%, the T_g decreased considerably. Also, T_g values in samples synthesized by free radical method were lower than those in samples synthesized by RAFT method.

References

1. Roghani-Mamaqani H, Haddadi-Asl V, Najafi M, Salami-Kalajahi M (2010) Synthesis and characterization of clay dispersed polystyrene nanocomposite via atom transfer radical polymerization. Polym Compos 31:1829–1837
2. Motahari S, Dornajafi L, Fotovat-Ahmadi I (2012) Migration of organic compounds from PET/clay nanocomposites: influences of clay type, content and dispersion state. Iran Polym J 21:669–681
3. Hajibaba A, Naderi G, Ghoreishy M, Bakhshandeh G, Razavi Nouri M (2012) Effect of single-walled carbon nanotubes on morphology and mechanical properties of NBR/PVC blends. Iran Polym J 21:505–511
4. Rahimi-Razin S, Haddadi-Asl V, Salami-Kalajahi M, Behboodi-Sadabad F, Roghani-Mamaqani H (2012) Matrix-grafted multi-walled carbon nanotubes/poly(methyl methacrylate) nanocomposites synthesized by in situ RAFT polymerization: a kinetic study. Int J Chem Kinet 44:555–569
5. Salami-Kalajahi M, Haddadi-Asl V, Rahimi-Razin S, Behboodi-Sadabad F, Najafi M, Roghani-Mamaqani H (2012) A study on the properties of PMMA/silica nanocomposites prepared via RAFT polymerization. J Polym Res 19: Article No. 9793
6. Ispas C, SokolovI Andreescu S (2009) Enzyme-functionalized mesoporous silica for bioanalytical applications. Anal Bioanal Chem 393:543–554
7. Ma X-H, Xu Z-L, Wu F, Xu H-T (2012) PFSA-TiO_2(or Al_2O_3)-PVA/PVA/PAN difunctional hollow fiber composite membranes prepared by dip-coating method. Iran Polym J 21:31–41
8. Khezri K, Haddadi-Asl V, Roghani-Mamaqani H, Salami-Kalajahi M (2012) Nanoclay-encapsulated polystyrene microspheres by reverse atom transfer radical polymerization. Polym Compos 33:990–998
9. Khezri K, Haddadi-Asl V, Roghani-Mamaqani H, Salami-Kalajahi M (2012) Synthesis of well-defined clay encapsulated poly (styrene-*co*-butyl acrylate) nanocomposite latexes via reverse atom transfer radical polymerization in miniemulsion. J Polym Eng 32:111–119
10. Jaymand M (2011) Surface modification of montmorillonite with novel modifier and preparation of polystyrene/montmorillonite nanocomposite by in situ radical polymerization. J Polym Res 18:957–963
11. Rahimi-Razin S, Haddadi-Asl V, Salami-Kalajahi M, Behboodi-Sadabad F, Roghani-Mamaqani H (2012) Properties of matrix-grafted multi-walled carbon nanotube/poly(methyl methacrylate) nanocomposites synthesized by in situ reversible addition-fragmentation chain transfer polymerization. Int J Chem Kinet 44:555–569
12. Duan J, Shao S, Li Y, Wang L, Jiang P, Liu B (2012) Polylactide/graphite nanosheets/MWCNTs nanocomposites with enhanced mechanical, thermal and electrical properties. Iran Polym J 21:109–120
13. Salami-Kalajahi M, Haddadi-Asl V, Behboodi-Sadabad F, Rahimi-Razin S, Roghani-Mamaqani H (2012) Properties of PMMA/carbon nanotubes nanocomposites prepared by "grafting through" method. Polym Compos 33:215–224
14. Jafarkhani M, Fazlali A, Moztarzadeh F, Mozafari M (2012) Mechanical and structural properties of polylactide/chitosan scaffolds reinforced with nano-calcium phosphate. Iran Polym J 21:713–720
15. Kresge CT, Leonowicz ME, Roth WJ, Vartuli JC, Beck JS (1992) Ordered mesoporous molecular sieves synthesized by a liquid-crystal template mechanism. Nature 359:710–712
16. Beck JS, Vartuli JC, Roth WJ, Leonowicz ME, Kresge CT, Schmitt KD, Chu CTW, Olson DH, Sheppard EW, McCullen SB, Higgins JB, Schlenker JL (1992) A new family of mesoporous molecular sieves prepared with liquid crystal templates. J Am Chem Soc 114:10834–10843
17. Choi JS, Kim DJ, Chang SH, Ahn WS (2003) Catalytic applications of MCM-41 with different pore sizes in selected liquid phase reactions. Appl Catal A-Gen 254:225–237
18. Selvaraj M, Pandurangan A, SeshadriK S, Sinaha PK, LalK B (2003) Synthesis, characterization and catalytic application of MCM-41 mesoporous molecular sieves containing Zn and Al. Appl Catal A-Gen 242:347–364
19. Grün M, Lauer I, Unger KK (1997) The synthesis of micrometer- and submicrometer-size spheres of ordered mesoporous oxide MCM-41. Adv Mater 9:254–257
20. Wight AP, Davis ME (2002) Design and preparation of organic-inorganic hybrid catalysts. Chem Rev 102:3589–3614
21. Jiamwijitkul S, Jongsomjit B, Praserthdam P (2007) Effect of Boron-modified MCM-41-supported dMMAO/zirconocene catalyst on copolymerization of ethylene/1-octene for LLDPE synthesis. Iran Polym J 16:549–559

22. Nejabat GR, Nekoomanesh M, Arabi H, Emami M, Aghaei-Nieat M (2010) Preparation of polyethylene nano-fibres using rod-like MCM-41/$TiCl_4$/$MgCl_2$/THF bi-supported Ziegler-Natta catalytic system. Iran Polym J 19:79–87
23. Hui S, Chattopadhyay S, Chaki TK (2010) Thermal and thermo-oxidative degradation study of a model LDPE/EVA based TPE system: effect of nano silica and electron beam irradiation. Polym Compos 31:1387–1397
24. Roghani-Mamaqani H, Haddadi-Asl V, Salami-Kalajahi M (2012) In situ controlled radical polymerization: a review on synthesis of well-defined nanocomposites. Polym Rev 52:142–188
25. Salami-Kalajahi M, Haddadi-Asl V, Behboodi-Sadabad F, Rahimi-Razin S, Roghani-Mamaqani H (2012) Effect of silica nanoparticle loading and surface modification on the kinetics of RAFT polymerization. J Polym Eng 32:13–22
26. Salami-Kalajahi M, Haddadi-Asl V, Ganjeh-Anzabi P, Najafi M (2011) Dithioester-mediated RAFT polymerization: a kinetic study by mathematical modeling. Iran Polym J 20:459–478
27. Salami-Kalajahi M, Haddadi-Asl V, Behboodi-Sadabad F, Rahimi-Razin S, Roghani-Mamaqani H, Hemmati M (2012) Effect of carbon nanotubes on the kinetics of in situ polymerization of methyl methacrylate. Nano 07:Article No. 1250003
28. Grun M, Unger KK, Matsumoto A, Tsutsumi K (1999) Novel pathways for the preparation of mesoporous MCM-41 materials—control of porosity and morphology. Micropor Mesopor Mater 27:207–216
29. Lai JT, Filla D, Shea R (2002) Functional polymers from novel carboxyl-terminated trithiocarbonates as highly efficient RAFT agents. Macromolecules 35:6754–6756
30. Salami-Kalajahi M, Haddadi-Asl V, Rahimi-Razin S, Behboodi-Sadabad F, Roghani-Mamaqani H, Hemmati M (2011) Investigating the effect of pristine and modified silica nanoparticles on thekinetics of methyl methacrylate polymerization. Chem Eng J 174:368–375
31. Rahimi-Razin S, Salami-Kalajahi M, Haddadi-Asl V, Roghani-Mamaqani H (2012) Effect of different modified nanoclays on the kinetics of preparation and properties of polymer-based nanocomposites. J Polym Res 19: Article No. 9954
32. Khezri K, Haddadi-Asl V, Roghani-Mamaqani H, Salami-Kalajahi M (2011) Synthesis and characterization of exfoliated poly(styrene-*co*-methyl methacrylate) nanocomposite via mini-emulsion atom transfer radical polymerization: an activators generated by electron transfer approach. Polym Compos 32:1979–1987
33. Perrier S, Barner-Kowollik C, Quinn JF, Vana P, Davis TP (2002) Origin of inhibition effects in the reversible addition fragmentation chain transfer (RAFT) polymerization of methyl acrylate. Macromolecules 35:8300–8306
34. Favier A, Charreyre MT, Pichot C (2004) A detailed kinetic study of the RAFT polymerization of a bi-substituted acrylamide derivative: influence of experimental parameters. Polymer 45:8661–8674
35. Arita T, Buback M, Vana P (2005) Cumyl dithiobenzoate mediated RAFT polymerization of styrene at high temperatures. Macromolecules 38:7935–7943
36. Blas H, Save M, Boissi E, Sanchez C, Charleux B (2011) Surface-initiated nitroxide-mediated polymerization from ordered mesoporous silica. Macromolecules 44:2577–2588
37. Singha S, Thomas MJ (2008) Dielectric properties of epoxy nanocomposites. IEEE T Dielect El In 15:12–23
38. Ash BJ, Schadler LS, Siegel RW (2002) Glass transition behavior of alumina/polymethylmethacrylate nanocomposites. Mater Lett 55:83–87
39. Tsagaropoulos G, Eisenberg A (1995) Dynamic mechanical study of the factors affecting the two glass transition behavior of filled polymers. Similarities and differences with random ionomers. Macromolecules 28:60–67